http://dx.doi.org/10.5012/bkcs.2011.32.11.3952

The Sintering Temperature Effect on Electrochemical Properties of $LiMn_2O_4$

Jin Tae Hwang, Sung Bin Park, Chang Kyoo Park, and Ho Jang*

*Department of Materials Science and Engineering, Korea University, Seoul 136-713, Korea. *E-mail: hojang@korea.ac.kr*
Received July 6, 2011, Accepted September 10, 2011

The effect of sintering temperature on the electrochemical property of $LiMn_2O_4$ was investigated. Results showed that the particle size was increased at higher sintering temperatures while the initial capacity was decreased after high temperature sintering. Capacity fading, on the other hand, was suppressed at lower sintering temperatures since the sintering at higher temperatures (≥ 800 °C) increased the Mn ions with a lower oxidation state (Mn^{+3}), which induced structural instability during cycling due to dissolution of Mn ions into the electrolyte. In particular, $LiMn_2O_4$ sintered above 830 °C showed severe capacity fading (capacity loss was 38% of initial capacity) by lower coulombic efficiency due to the abnormally increased particle size.

Key Words : $LiMn_2O_4$, Manganese dissolution, Capacity fading, Sintering, Particle size

Introduction

The lithium secondary battery in a portable electronic device has attracted major attention as a key component since its commercial application two decades ago. This is because the recyclable power source can determine the size, shape, weight, function and life span of portable devices. In addition, lithium secondary batteries have drew more attention after the commercialization of the electric vehicles powered by rechargeable batteries. A large amount of research and development efforts have been devoted to improve the lithium based secondary batteries concerning the capacity, sustainability, safety, eco-friendliness, and cost reduction.

In the development of rechargeable batteries, considerable effort has been given to improve the electrochemical properties of the cathode because it plays a key role in determining the above mentioned requirements. Currently, the cathodes used in commercial lithium secondary batteries are based on $LiCoO_2$, even though it suffers from high material cost, toxicity of cobalt, and microcracks caused by the volume change during the charge-discharge cycles. As an alternative, $LiMn_2O_4$ with a spinel structure has been considered as a next generation rechargeable battery.[1] This is because $LiMn_2O_4$ shows good safety and high discharge voltage in addition to its non-toxicity and low cost.[2-4] On the other hand, $LiMn_2O_4$ shows rapid capacity fading during cycling and the early capacity loss makes the large scale commercial development difficult. The main causes of the early capacity fade are associated with the oxygen deficiency of $LiMn_2O_4$ crystals,[5] structural transformation with Jahn-Teller distortion near 3.2 V during cycling,[6] and Mn dissolution due to the reactive electrolyte.[7]

In particular, the oxygen deficiency in $LiMn_2O_4$ is known to aggravate the electrochemical properties more when the particle is heat treated at high temperatures.[8] It induces a change in the mean charge state of the Mn ion, alters the lattice parameter, and deteriorates the electrical properties.[9,10] On the other hand, Mn dissolution reduces the amount of active materials after a reaction with the electrolyte, which is represented by the Hunter's reaction[11]; $2LiMn_2O_4 + 4H^+ = 3\lambda\text{-}MnO_2 + Mn^{+2} + 2Li^+ + 2H_2O$. The proton in the chemical reaction is supplied as a byproduct of the chemical reaction of $LiPF_6$ in the electrolyte and water molecules, and Mn^{+2} ions are produced from the reaction; $2Mn^{+3} = Mn^{+2} + Mn^{+4}$. The $\lambda\text{-}MnO_2$ phase in the reaction is electrochemically inert because the protons are bound strongly by the oxygen ions around the Mn vacancy in a 16d position. Another kinetic barrier for Li ion diffusion is the presence of a solid electrolyte interface (SEI) on the $LiMn_2O_4$ particle surface, which is produced by the reaction of $LiMn_2O_4$ and the electrolyte.[12,13] The large contact surface between the active particles and electrolyte decreases the capacity retention due to Mn dissolution.[14,15]

The heat treatment temperature also plays a key role in the electrochemical properties of $LiMn_2O_4$. This is because the heat treatment temperature affects the particle surface area, morphology, size distribution, and the oxygen deficiency,[5] which is known to decrease the cycle performance,[8] whereas its effect on the initial capacity is not significant.[16] Therefore, the optimum heat treatment temperature is important to achieve the best electrochemical performance of $LiMn_2O_4$.

In this study, the effect of sintering temperature on the electrochemical performance was investigated. The kinetics of particle growth was studied to determine the grain growth mechanisms at the different temperature ranges. In particular, the causes of capacity fading were analyzed by examining the particle size, dissolution of the Mn ions, and lattice parameters.

Experimental

Materials. A sol-gel method was used to produce $LiMn_2O_4$ from lithium acetate dehydrate and manganese acetate tetrahydrate mixed in acrylic acid. The molar ratio of the Li source, Mn source, and acrylic acid was 1:2:6. The

Table 1. The designation of $LiMn_2O_4$ samples and their heat treatment temperature

Symbol	Heat treatment temperature (°C)
LMO600	600
LMO700	700
LMO800	800
LMO830	830
LMO870	870

precursors were mixed in distilled water using a magnetic stirrer for 30 min. The solution was dried at 80 °C for 7 days and ground to produce a precursor. The precursor was heat treated at two different temperatures to produce $LiMn_2O_4$ containing Mn^{+3} and Mn^{+4} ions at a 1:1 ratio while completely removing organic volatiles. The low temperature treatment was used to produce embryonic $LiMn_2O_4$ particles by providing sufficient time and the particles were grown to appropriate sizes with high crystallinity by the heat treatment at a higher temperature. Thermogravimetric analysis (TGA) of the precursor was carried out at 10 °C/min in an N_2 atmosphere. No weight change was observed beyond 600 °C, suggesting that all the volatiles had been removed. Therefore, the precursor was heat treated at 600 °C for 10 hours first and heat-treated again for 15 hours at temperatures ranging from 700 °C to 870 °C (Table 1). The battery sample was produced first by casting a slurry (active material: acetylene black: polyvinylidene difluoride = 85:10:5 wt %) onto Al foil. The slurry was then dried to produce a cathode and was assembled with an electrolyte (ethylene carbonate: dimethyl carbonate: ethylmethyl carbonate = 1:1:1 vol % with 1M $LiPF_6$) and a Li metal anode to produce coin cell batteries.

Analysis. The crystal of $LiMn_2O_4$ was examined by X-ray diffraction (Rigaku D/MAX-2500V/PC, Cu Kα, 40 kV, 50 mA). The grain size of the particle was obtained from the full width at half maximum (FWHM) of 7 high intensity peaks using Scherrer's formula. The mean particle size was also measured by scanning electron microscopy (SEM, Hitachi S-4300, Japan) by randomly selecting 100 particles using an image analyzer. The surface area of the particle was obtained by Brunauer-Emmett-Teller (BET, ASAP2010) analysis. The electrochemical performance of the coin cell was evaluated using a battery cycler (Maccor4000, Maccor) in the range of 3.5-4.5 V at 0.5 C for 50 cycles.

Results and Discussion

Structure and Morphology. The microstructure of $LiMn_2O_4$ produced by the heat treatment at different temperatures was examined by X-ray diffraction (Fig. 1). The figure shows that the $LiMn_2O_4$ produced at 600 °C contains a secondary phase, such as Mn_2O_3 and a fully crystallized spinel structure was achieved when the heat treatment was performed at temperatures higher than 600 °C. The mean grain size, calculated using Scherrer's formula, increased with increasing temperature (Table 2). A similar result was reported by Hwang *et al.*, who showed a comparable grain size after heat treatment at 800 °C.[17]

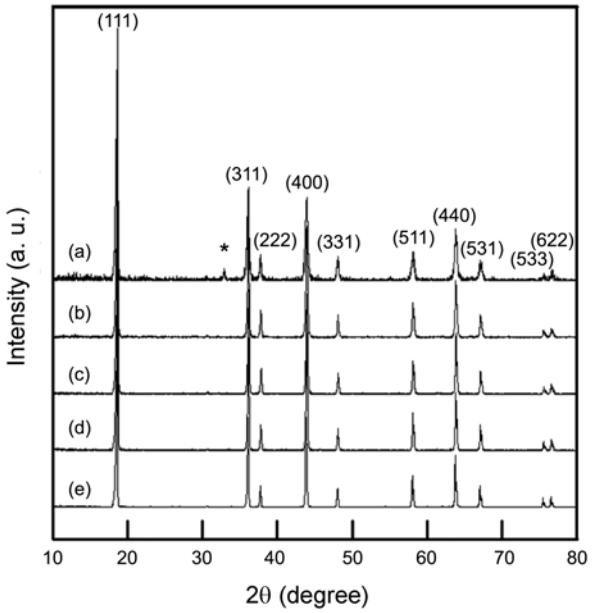

Figure 1. X-ray diffraction patterns of $LiMn_2O_4$ heat treated at different temperatures; (a) LMO600, (b) LMO700, (c) LMO800, (d) LMO830, (e) LMO870. *indicates the peaks correnponding to Mn_2O_3 phase.

The particle morphology was also examined by SEM. Figure 2 shows SEM images of the heat treated particles produced at different temperatures. The particles were faceted and the size distribution was wider when they were produced at high temperatures. The mean particle size in the SEM images was calculated from 100 particles using an image analyzer (Table 2). The particle size increased with increasing sintering temperature. On the other hand, the particle size estimated from the SEM images were much larger than the sizes calculated from the Scherrer's formula, suggesting that the particles were polycrystals after the heat treatment.[3]

The abrupt increase in particle size at high temperatures was examined by plotting Arrhenius type curves because the particle size is determined mainly by a diffusional kinetic process (Fig. 3). From the relationship between grain growth and temperature,[18] the grain size (D) after heat treatment was presented using the following equation (Eq. 1);

Table 2. The average grain size and particle diameter, BET area, and lattice parameter of $LiMn_2O_4$

Heat treatment temperature (°C)	Average grain size (nm)	Average particle diameter (μm)	BET area (m_2/g)	Lattice parameter (Å)
600	26.97	0.345	-	-
700	29.67	0.428	-	8.2486
800	40.14	0.878(± 0.05)	0.9903	8.2635
830	52.32	1.546(± 0.09)	0.5939	8.2662
870	55.79	3.352(± 0.32)	0.3508	8.2657

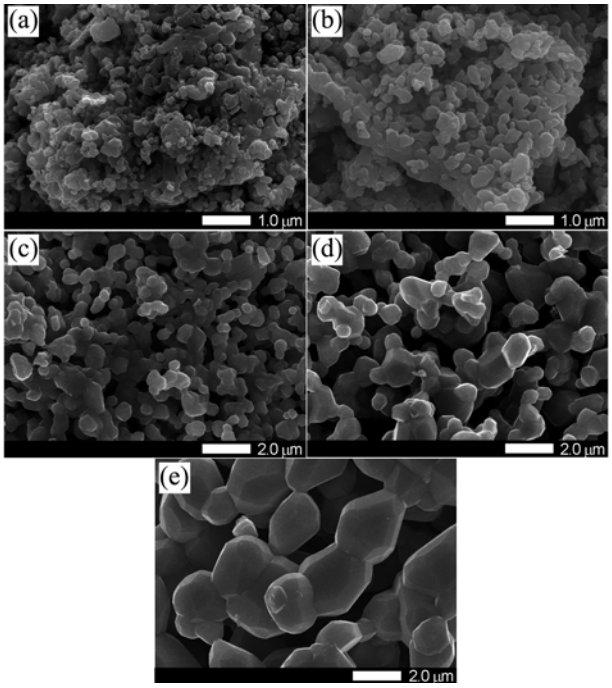

Figure 2. SEM micrographs of $LiMn_2O_4$ particles obtained from (a) LMO600, (b) LMO700, (c) LMO800, (d) LMO830, (e) LMO870.

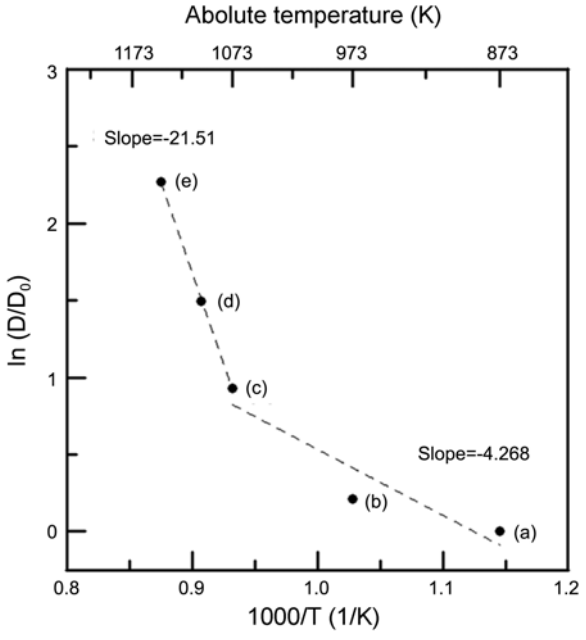

Figure 3. Arrhenius type plot indicating two different growth mechanisms at different temperature ranges; (a) LMO600, (b) LMO700, (c) LMO800, (d) LMO830, (e) LMO870.

$$D = D_o \exp\left(-\frac{Q}{RT}\right) \quad (1)$$

where Q is the activation energy associated with the particle growth process and D_o is the initial size of the particle. Calculated from the slopes in Figure 3, the activation energies at the low temperature and high temperature ranges

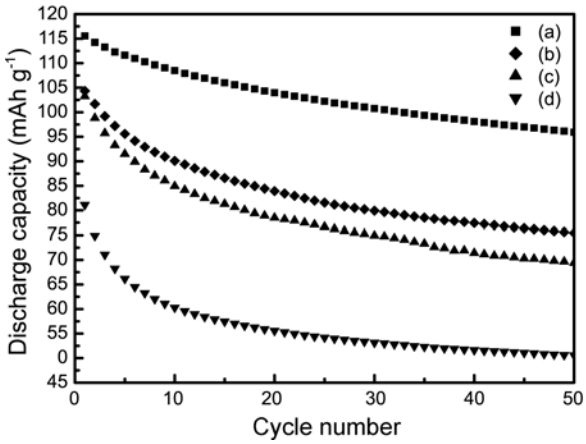

Figure 4. The discharge capacity changed during cycling tests using (a) LMO700, (b) LMO800, (c) LMO830, (d) LMO870.

were 35 kJ/mole and 169 kJ/mole, respectively, and the transition temperature was approximately 800 ºC. This suggests that the particle growth mechanism is different when the heat treatment is performed at different temperatures. The high activation energy associated with the high temperature process is attributed to bulk diffusion, whereas at low temperatures, grain growth is dominated by surface diffusion.[19-22]

The specific surface area of the particle was obtained by BET measurements. A large specific surface area was obtained from the smaller particles (Table 2). The specific surface area is an important parameter in determining the electrochemical properties of $LiMn_2O_4$ because the particle surface is a gateway for Li ion transfer during the charge-discharge cycles and for Mn dissolution.[23,24]

Electrochemical Properties. The performance of the $LiMn_2O_4$ particles sintered at different temperatures was examined by repeating the charge-discharge cycles 50 times in the range of 3.5-4.5 V at 0.5 C at room temperature. The initial capacity and capacity fading were strongly affected by the sintering temperature, as shown in Figure 4. The initial capacity of $LiMn_2O_4$ particles sintered at the lowest temperature was 115 mAh/g, whereas the $LiMn_2O_4$ particles sintered at the highest temperature showed only 81 mAh/g.

The higher initial capacity of the $LiMn_2O_4$ sintered at lower temperature in Table 3 was attributed to the increased surface area contacted with the electrolyte. Jang *et al.*[23] reported similar results showing better discharge capacity from small and uniform particles. Momchiov *et al.*[24] also reported that the heat treatment temperature changed the total surface area of the particles and affected the electrochemical properties of $LiMn_2O_4$. The extent of particle agglomeration, which interrupted the surface contact with electrolyte, was examined by cleaning the cathode after cycle tests using dimethyl carbonate. Figure 5 shows SEM images obtained from the cathode surface containing $LiMn_2O_4$ particles sintered at different temperatures. In the case of small $LiMn_2O_4$ particles, the active materials were distributed homogeneously and well mixed with acetylene black, whereas the large $LiMn_2O_4$ particles were agglomerat-

Table 3. Charge-discharge characteristics of LMO700, LMO800, LMO830, LMO870

Cathode	Sintering Tem. (°C)	Ave. diameter (μm)	1st discharge capacity (mAh/g)	50th discharge capacity (mAh/g)	Capacity retention (%)	Sum of Δredox peaks (V) (50th cycle)
LMO700	700	0.428	115.55	95.9	83	0.0677
LMO800	800	0.878	104.33	75.49	72	0.1311
LMO830	830	1.546	103.23	69.42	67	0.1327
LMO870	870	3.352	81.12	50.56	62	0.1738

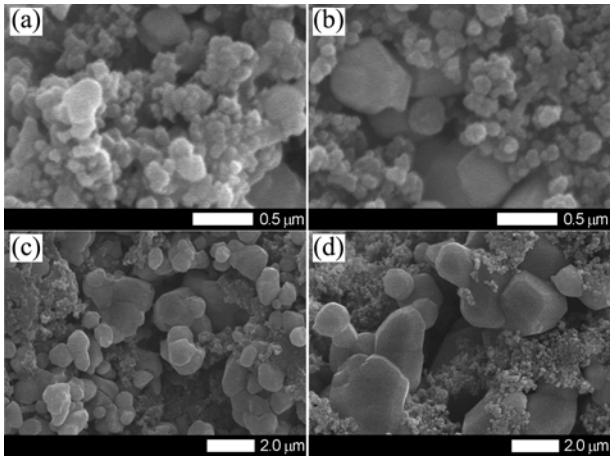

Figure 5. SEM micrographs of the cathode surface after 50 cycles; (a) LMO700, (b) LMO800, (c) LMO830, (d) LMO870. The cathode was cleaned with dimethyl carbonate and dried.

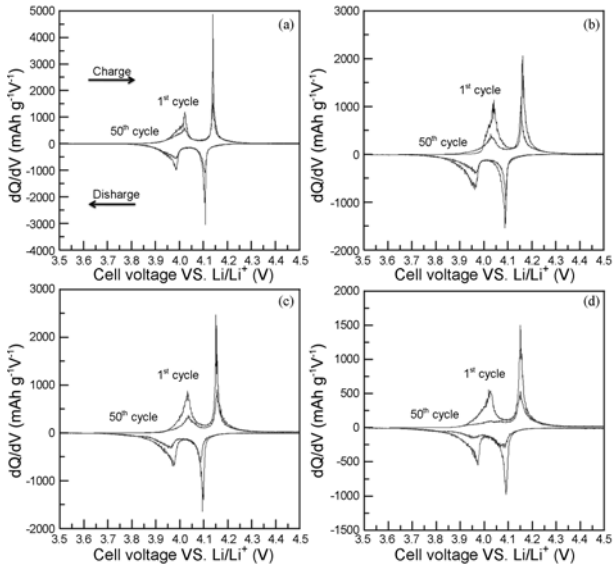

Figure 6. The dQ/dV plotted as a function of cell voltage measured during 1st and 50th cycles using coin cells produced by (a) LMO700, (b) LMO800, (c) LMO830, (d) LMO870.

ed and poorly mixed with acetylene black. These results suggest that the initial capacity of the large $LiMn_2O_4$ particles is inferior to that of small ones because of the smaller effective area, lower electrical conductivity of electrode, and longer diffusion path of Li ion.[3]

The capacity retention after 50 cycles was also affected by the sintering temperature, showing approximately 83% capacity retention after 50 cycles in the case of using LMO700. On the other hand, LMO870 retained only 62% after 50 cycles, indicating that much better fade resistance can be achieved by lower temperature sintering. The differential capacity (dQ/dV) was plotted as a function of the cell potential (V) to compare redox potentials from different particle sizes (Fig. 6). The peak difference in the figure, which was the sum of the differences from the two peaks observed during charge and discharge, indicates the amount of the polarization built up during a cycle test. The redox peaks were found near 4 V and 4.15 V and the difference in the redox peaks of LMO870 obtained from the 50th cycle was significantly larger than that of LMO700, suggesting that higher polarization was obtained by sintering at higher temperatures. Table 3 summarizes the charge-discharge characteristics obtained from the $LiMn_2O_4$ particles produced at different heat treatment temperatures.

To examine the main causes of the capacity fade of the particles sintered at higher temperatures, the relationship between the effective surface area of the particles and Mn dissolution was investigated by comparing the thermal decomposition of the SEI layers on the particles after impregnating them in the electrolyte at 80 °C for 5 days. This is because the capacity retention of $LiMn_2O_4$ can be affected by the amount of Mn dissolution.[1,25] Thermogravimetric analysis (TGA) and differential scanning calorimetry (DSC) were used to compare the SEI layers produced on the particle surface during impregnation. Figure 7 shows the results of TGA and DSC analysis when the $LiMn_2O_4$ particles produced at 800 °C were reacted with the electrolyte(a) and pristine $LiMn_2O_4$(b). The results showed that the particles reacted with the electrolyte showed a different thermal decomposition temperature compared to the unreacted one. The particles reacted with the electrolyte showed exothermic peaks at three different temperature ranges at 25-30 °C (peak 1), 30-150 °C (peak 2), and 150-270 °C (peak 3), respectively. On the other hand, the particles without impregnation exhibited peak 1 only. The peak 1 appeared near 25 °C and was assigned to the phase transition of $LiMn_2O_4$, which was associated with Jahn-Teller distortion.[26] On the other hand, two other peaks at higher temperature ranges indicated the thermal decomposition of the reaction product on the particle surface. The solid electrolyte interface (SEI) on the particle surface was produced by a chemical reaction of the electrolyte with the $LiMn_2O_4$ particles and was decomposed at elevated temperatures.[27] Peak 2 in Figure 7(a) was produced by the exothermic decomposition of SEI and was accompanied by

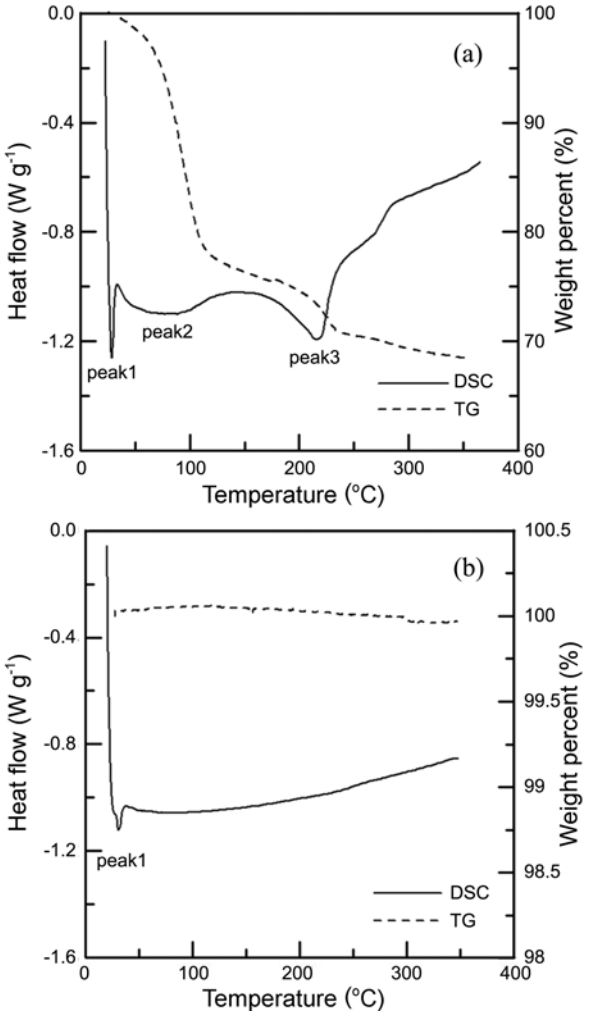

Figure 7. Heat flow and weight change of the $LiMn_2O_4$ particles (LMO800); (a) impregnated with the electrolyte at 80 °C for 5 days and dried, (b) without impregnation.

approximately 30% weight reduction, whereas only 5% of the weight reduction was observed in peak 3. Table 4 compares the amount of heat flow during DSC analysis. Large specific surface area results in more large contact area with electrolyte. The integrated peak area from peak 2 and peak 3 describes the amount of SEI on the particle surface since the heat flow is due to thermal decomposition of the SEI. The table shows that the amount of heat flow from LMO870 is much smaller than that of LMO800, which agrees well with the relatively small specific surface area.

On the other hand, the results from the room temperature charge-discharge experiments in Table 3 indicate that the capacity retention of the smaller particles is better than larger particles, suggesting that the factors other than the surface area play important roles in determining the capacity retention. One of the possible causes for this contradictory finding appears to be the difference in the relative amount of Mn ions (Mn^{2+}, Mn^{3+}, Mn^{4+}) in the $LiMn_2O_4$ particles when produced at different temperatures.[10] To investigate the oxidation state of Mn ions in the $LiMn_2O_4$ particles, the lattice parameter of LMO700, LMO 800, LMO 830, and LMO870 was calculated from the XRD data (Table 2). The lattice parameter tended to increase at higher temperatures, whereas the lattice parameters from the particles produced at > 800 °C did not change considerably with the heat treatment temperature. Similar results were reported by other researchers.[8,28]

The increase in the lattice parameters of $LiMn_2O_4$ particles produced at high temperatures is associated with oxygen vacancies in the lattice.[8] This is because the number of oxygen vacancies increases with increasing the heat treatment temperature, accompanied by a decrease in the average oxidation state of the Mn ions.[9,15,28] In the case of $LiMn_2O_4$, Mn^{3+} and Mn^{4+} ions are located in the octahedral site in high spin states[29] and the ionic radius of Mn^{3+} is greater than

Table 4. The specific surface area and total heat flow obtained during DSC analysis using LMO800 and LMO870 impregnated with electrolyte

Sintering temperature (°C)	Specific surface area (m^2/g)	Integrated area for peak2+peak3 (J/g)
800	0.9903	-146.1
870	0.3508	-61.6

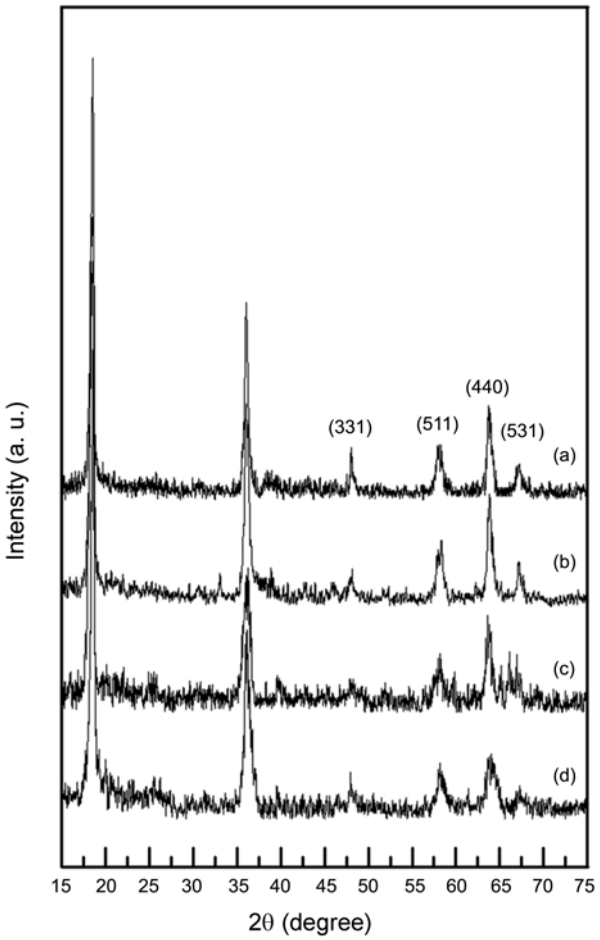

Figure 8. XRD patterns obtained after charge-discharge tests repeated 50 time using (a) LMO700, (b) LMO800, (c) LMO830, (d) LMO870.

Mn^{4+}.[30] G.G. Amatucci *et al*. reported that the lattice parameter of $LiMn_2O_4$ was increased when the average oxidation state of Mn was decreased.[26] This suggests that the axial length of MnO_6 was greater with Mn^{3+} than Mn^{4+}. Therefore, the increased lattice parameter of the $LiMn_2O_4$ particles produced at 800 °C is due to the increase in Mn^{3+} ion concentration in the lattice, whereas the similar lattice parameters of LMO800, LMO830, and LMO870 suggest little influence on the Mn^{3+}/Mn^{4+} ratio. The dissolution of Mn ions into the electrolyte follows the reaction; $2Mn^{3+}(solid) = Mn^{4+}(solid) + Mn^{2+}(solution)$. Therefore, a larger amount of Mn^{3+} in the $LiMn_2O_4$ calcined at 800 °C is responsible for the poor capacity retention.

To confirm Mn dissolution of the $LiMn_2O_4$ particles produced at high temperatures, the XRD patterns were compared after 50 charge-discharge tests (Fig. 8). The figure shows lower and broader intensity peaks near (331), (511), (440) and (531) planes from the particles produced at higher temperatures. This is consistent with the XRD data obtained after Mn dissolution by impregnating the cathode with the electrolyte[13] and is similar to the XRD pattern when Li ions are introduced into Mn vacancies in the 16d position in the lattice.[6] Figure 8 also shows the XRD peaks corresponding to λ-MnO_2 when the charge-discharge tests were carried out using $LiMn_2O_4$ particles produced at high temperatures,[31] indicating that an irreversible structural change takes place in the lattice after Mn dissolution.

However, the XRD patterns from LMO830 and LMO870 in Figure 8 were similar and the lattice parameters of the $LiMn_2O_4$ particles sintered at the tempreature higher than 800 °C were similar (Table 2. LMO800, LMO830, LMO870). These results indicate that the lower capacity retention of LMO830 and LMO870 is attributed to the other factors in addition to Mn dissolution. To investigate this observation, the coulombic efficiency of LMO700, LMO800, LMO870 was examined (Fig. 9). The figure shows that the coulombic efficiency of LMO700 and LMO800 were about 99% after 25 cycles, while that of LMO870 was 98% after 15 cycles with much lower coulombic efficiency at earlier cycles. The reduction of coulombic efficiency of LMO870 is attributed to the significantly increased particle size (Table 2, Fig. 5), causing inhomogeneous mixing with carbon conductors and reduction of the specific surface area. This is consistent with the previous results by Lu *et al*.[32] They reported that a large particle size reduced the specific surface area and coulombic efficiency, simultaneously. Only one percentage difference in coulombic efficiency can change capacity retention significantly, because the capacity retention is exponentially proportional to the coulombic efficiency (Eq. 2).

$$\text{Capacity retention} \propto Q^N \quad (2)$$

Q: coulombic efficiency, N: number of cycle

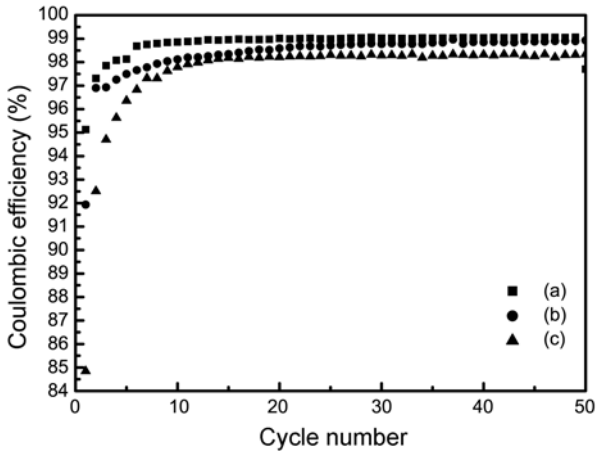

Figure 9. Coulombic efficiency calculated during cycle tests using (a) LMO700, (b) LMO800, (c) LMO870.

Conclusions

The sintering temperature effect of $LiMn_2O_4$ on the electrochemical property was examined by changing the heat treatment temperature and the results are summarized as follows;

(1) The particle size increased when heat treatment was performed at higher temperatures. The particles were coarsened significantly at the temperatures higher than 800 °C and large particles exhibited a broad size distribution and agglomeration.

(2) The $LiMn_2O_4$ particles produced at elevated temperatures showed low initial capacity, which was caused by particle coarsening, inhomogeneous mixing with the conductor, and reduced contact area with the electrolyte.

(3) Capacity retention during the cycle test was decreased in the case of the larger $LiMn_2O_4$ particles produced at higher heat treatment temperatures. Contact area with electrolyte was not a main factor for capacity fading, when electrically cycled at room temperature.

(4) Poor capacity retention of $LiMn_2O_4$ particles sintered at above 800 °C was attributed to the increase in Mn^{3+}/Mn^{4+} ratio induced by oxygen deficiency and accompanying Mn dissolution. Capacity fading of $LiMn_2O_4$ particles heat treated above 830 °C was due to additional lower coulombic efficiency from the large particle size.

Acknowledgments. This work was financially supported by a grant from the Korean Ministry of Knowledge Economy (Research grant code #: 2008EEL11P0800002009).

References

1. Fergus, J. W. *J. Power Sources* **2010**, *195*, 939.
2. Taniguchi, I.; Lim, C. K.; Song, D.; Wakihara, M. *Solid State Ionics* **2002**, *146*, 239.
3. Singhal, R.; Resto, O.; Katiyar, R. S. *J. Renewable and Sustainable Energy* **2009**, *1*, 023103-1.
4. Yi, T. F.; Hu, X. G.; Dai, C. S.; Gao, K. *J. Master Sci.* **2007**, *42*, 3825.
5. Wang, X. Q.; Nakamura, H.; Yoshio, M. *J. Power Sources* **2002**, *110*, 19.
6. Gummow, R. J.; de Kock, A.; Thackeray, M. M. *Solid State Ionics* **1994**, *69*, 59.
7. Jang, D. H.; Shin, Y. J.; Oh, S. M. *J. Electrochem. Soc.* **1996**, *143*,

2204.
8. Lee, Y. S.; Hideshima, Y.; Sun, Y. K.; Yoshio, M. *J. Electroceramics* **2002**, *9*, 209.
9. Yonemura, M.; Yamada, A.; Kobayashi, H.; Tabuchi, M.; Kamiyama, T.; Kawamoto, Y.; Kanno, R. *J. Mater. Chem.* **2004**, *14*, 1948.
10. Sugiyama, J.; Atsumi, T.; Koiwat, A.; Sasaki, T.; Hioki, T.; Noda, S.; Kamegashira, N. *J. Phys: Condens. Matter.* **1997**, *9*, 1729.
11. Park, S. B.; Shin, H. C.; Lee, W. G.; Cho, W. I.; Jang, H. *J. Power Sources* **2008**, *180*, 597.
12. Zhang, S. S.; Xu, K.; Jow, T. R. *J. Electrochem. Soc.* **2002**, *149*, A1521.
13. Du Pasquier, A.; Blyr, A.; Courjal, P.; Larcher, D.; Amatucci, G.; Gerand, B.; Tarascon, J. M. *J. Electrochem. Soc.* **1999**, *146*, 428.
14. Lu, C. H.; Saha, S. K. *Materials Science and Engineering B* **2001**, *79*, 247.
15. Xia, Y. Y.; Kumada, N.; Yoshio, M. *J. Power Sources* **2000**, *90*, 135.
16. Tarascon, J. M.; Wang, E.; Shokoohi, F. K.; McKinnon, W. R.; Colson, S. *J. Electrochem. Soc.* **1991**, *138*, 2859.
17. Hwang, B. J.; Santhanam, R.; Liu, D. G. *J. Power Sources* **2001**, *101*, 86
18. Wei, Y. J.; Kim, K. B.; Chen, G.; Park, C. W. *Materials Characterization* **2008**, *59*, 1196.
19. Aihara, K.; Chaklader, A. C. D. *ACTA Metallurgica*. **1975**, *23*, 855.
20. Hofmann, S.; Csanyi, G.; Ferrari, A. C.; Payne, M. C.; Robertson, J. *Physical Review Lett*. **2005**, *95*, 036101.
21. Jiang, Q.; Zhang, S. H.; Li, J. C. *Solid State Commun.* **2004**, *130*, 581.
22. Barsoum, M. W. *Fundamentals of Ceramics*; McGraw-Hill Book Companies: St Louis, 1997; pp 331-353.
23. Jang, S. W.; Lee, H. Y.; Shin, K. C.; Lee, S. M.; Lee, J. K.; Lee, S. J.; Baik, H. K.; Rhee, D. S. *J. Power Sources* **2000**, *88*, 274.
24. Momchilov, A.; Manev, V.; Nassalevska, A. *J. Power Sources* **1993**, *41*, 305.
25. Park, S. B.; Lee, S. M.; Shin, H. C.; Cho, W. I.; Jang, H. *J. Power Sources* **2007**, *166*, 219.
26. Amatucci, G. G.; Schmutz, C. N.; Blyr, A.; Sigala, C.; Gozdz, A. S.; Larcher, D.; Tarascon, J. M. *J. Power Source* **1997**, *69*, 11.
27. Richard, M. N.; Dahn, J. R. *J. Power Sources* **1999**, *79*, 135.
28. Son, J. T.; Park, K. S.; Kim, H. G. *J. Mater. Science* **2004**, *39*, 3635.
29. Nakayama, M.; fNogami, M. *Solid State Commun.* **2010**, *150*, 1329.
30. Shannon, R. D. *Actacrystallographica. Section A* **1976**, *32*, 751.
31. Raveendranath, K.; Ravi, J.; Jayalekshmi, S.; Rasheed, T. M. A.; Nair, K. P. R. *Mater. Sci. Eng. B* **2006**, *131*, 210.
32. Lu, C. H.; Lin, S. W. *J. Power Sources* **2001**, *97-98*, 458.